Electronic Couplings for Charge Transfer across Molecule/Metal and Molecule/Semiconductor Interfaces: Performance of the Projector Operator-Based Diabatization Approach

Zdenek Futera[1] and Jochen Blumberger[1,2]*

[1]University College London, Department of Physics and Astronomy,

Gower Street, London WC1E 6BT, UK

[2]Institute for Advanced Study, Technische Universität München, Lichtenbergstrasse 2 a,

D-85748 Garching, Germany

Abstract

One principal parameter determining charge transfer rates between molecules and metals is the electronic coupling strength between the discrete electronic states of the molecule and the band states of the metal. Their calculation with computational chemistry methods remains challenging, both conceptually and in practice. Here, we report the implementation of the projection-operator diabatization (POD) approach of Kondov *et al.* (*J. Phys. Chem. C* **2007**, *111*, 11970-11981.) in the CP2K program package, which extends the range of applications to charge transfer at infinite periodic surfaces. In the POD approach the self-consistent Kohn-Sham Hamiltonian of the full

---

[*] Corresponding authors: j.blumberger@ucl.ac.uk, z.futera@ucl.ac.uk; Tel: ++44-(0)20-7679-4373 (JB), Fax: ++44-(0)20-7679-7145 (both)

system is partitioned in donor (e.g. molecule) and acceptor (e.g. metal) blocks which are block-diagonalized. The coupling matrix elements between donor and acceptor states are simply identified with the matrix elements of the off-diagonal block. We find that the POD method performs similarly well as constrained DFT (CDFT) on the HAB11 database for excess hole transfer between simple organic dimers, with a mean unsigned error of 14.0 meV, compared to 11.8 meV in CDFT. By studying two case examples, electron injection from a dye molecule to TiO_2 and electron transfer from a molecule, that forms self-assembled monolayers, to metallic Au(111), we demonstrate that the POD method is a useful and cost-effective tool for estimation of electronic coupling across heterogeneous interfaces.

I.   Introduction

Charge transfer reactions are ubiquitous in chemistry and biology. For example, electron-transfer (ET) chains in chloroplasts and in mitochondria are parts of fundamental biochemical processes of photosynthesis and respiration.[1-9] Moreover, redox processes are crucial for functioning of various metalloproteins and enzymes such as hemoglobin, plastocyanin, cytochromes or hydrogenase,[10-15] to name at least some of them. Besides charge-transport processes between redox species in liquid electrolytes, ET reactions across solid/liquid and solid/molecule interfaces are of great importance in electrochemistry, catalysis, energy materials research and molecular electronics[16-21].

  From a theoretical point of view, Marcus theory[22,23] is in most cases employed to describe electron transfer between charge localized or diabatic electronic states on electron donor and acceptor. In this theory the electronic coupling matrix element between the two diabatic states, on which we focus in the current study, is one of the principal parameters determining the ET rate. There are several different methods to construct diabatic states and calculate the corresponding electronic coupling matrix elements such as block diagonalization,[24,25] generalized Mulliken-Hush

method (GMT),[26,27] fragment charge difference,[28] fragment energy difference,[29] projection methods,[30,31] fragment orbital density functional theory (FODFT),[32-36] constrained density functional theory (CDFT)[37-40] and ultrafast parametrized methods.[41] While the *ab initio* wavefunction-based approaches are accurate but limited by their high computational cost to small molecules only, the less-demanding DFT methods are typically affected by self-interaction error of uncorrected exchange-correlation functionals.[42,43] In recent work, our group has compiled two ab-initio databases for electronic coupling matrix elements for transfer of an excess hole and excess electron in dimers of small π-conjugated organic molecules, denoted HAB11[44] and HAB7,[45] respectively. A comparison to high-level ab-initio wavefunction theory results showed that the more cost effective CDFT method performed best on π-conjugated organic molecules when a functional was used that contained about 50% Hartree-Fock exchange.

The CDFT method and its extension CDFT configuration interaction (CDFT-CI)[46] were designed to give electronic couplings between a few discrete molecular electronic states in the form of charge (or spin) localized Kohn-Sham determinants. Unfortunately, this approach becomes impractical for the modelling of heterogeneous ET across metallic interfaces, where electronic couplings to a large number of band states are needed. According to Marcus-Hush[47-50] theory for heterogeneous ET the rate constant is given by

$$k_{red/ox} = \frac{2\pi}{\hbar} \int H_{ab}^2(\varepsilon) \, f_\pm(\varepsilon, \varepsilon_F) \, \rho(\varepsilon) \, F(\varepsilon) \, d\varepsilon, \qquad (1)$$

where $f_\pm(\varepsilon, \varepsilon_F) = [1 + \exp(\pm(\varepsilon - \varepsilon_F)/k_B T)]^{-1}$ is Fermi-Dirac distribution function determining occupancies of metallic states ε with respect to system Fermi level ε_F and thermal energy $k_B T$. The plus sign in the exponential factor corresponds to reduction of the molecular state while the minus sign is used in case of oxidation. Further, $\rho(\varepsilon)$ is density of the metallic states and $F(\varepsilon) = (4\pi\lambda k_B T)^{-1/2} \exp[-(\varepsilon - \varepsilon_0 + \lambda + e\eta)^2/4\lambda k_B T]$ is the Frank-Condon

factor. Free energy barrier involved as an argument of the exponential in the last term depends on the energy difference between the donor molecular state ε_0 and the acceptor metallic state ε, reorganization free energy of the molecule λ and electrode overpotential η. Finally, energy-dependent electronic coupling elements H_{ab} between the molecular and metallic states are involved in the rate-constant integration. This suggests that methods that approximate electronic couplings as Hamiltonian matrix elements between 1-electron orbitals rather than Kohn-Sham determinants are more suitable for this purpose. Unfortunately, our FODFT method that belongs to the former category of methods is not suitable as it neglects interactions between donor and acceptor, which can be assumed to be large for molecules adsorbed on metallic surfaces (e.g. image charge effects).

Some time ago, Kondov et al.[51] suggested a simple and effective method to obtain electronic couplings for charge transfer of molecules adsorbed in surfaces. Starting from a standard Kohn-Sham DFT calculation on the whole system, the resultant self-consistent KS Hamiltonian is expressed in terms of an orthogonalized atomic orbital basis set and partitioned in donor and acceptor blocks, H_{AA} and H_{BB}. After separate diagonalization of donor and acceptor blocks, the matrix elements contained in the transformed off-diagonal blocks, H_{AB}, are identified as electronic couplings between the block-diagonal donor and acceptor states. More recently, Kastlunger and Stadler suggested three alternative methods for the calculation of coupling matrix elements in the context of the modelling of single molecule junctions.[21]

While the method of Kondov et al. was successfully applied to interfacial systems,[51-54] the performance of this method against high-level ab-initio data has not been assessed. Moreover, calculations were carried out only on finite cluster models of extended surfaces. Here we report on the implementation of this method, that we term ``projection-operator diabatization'' (POD), in the

CP2K simulation package,[55] thereby extending its range of applications to ET across periodic surfaces.[56-58] At first, we benchmark the method against high-level ab-initio data for simple interatomic and intermolecular electron transfer reactions in vacuum (HAB11 database).[39,44] We then apply the method to electron injection from an organic dye molecule to a TiO_2 nanoparticle[51] and to an extended surface of anatase TiO_2. We also investigate electron transfer from an organic molecule forming self-assembled monolayers to a periodic gold surface and compare to the finite cluster results of Prucker et al.[54]

We find that the POD method used in combination with a hybrid functional containing 50% exact exchange performs similarly well as CDFT on the HAB11 database, while providing a useful tool for investigation of the charge transfer kinetics on heterogeneous metallic or semiconducting interfaces. A challenging system where POD and CDFT give rather different results, hole tunneling between neutral and charged oxygen vacancy defects in bulk MgO,[59,60] are discussed at the end of the manuscript.

II.   Theory

Here, we describe the POD approach to electronic coupling calculations, which was introduced by Kondov et al.[51] In the Results and Discussion section that follows further below we compare our POD results with electronic couplings obtained from constrained density functional theory (CDFT)[37,38] and from fragment orbital density functional theory (FODFT).[33,34] For convenience, the latter two methods are briefly explained in the Supporting Information.

The POD method can be viewed as a post-processing Hamiltonian-partitioning approach that starts from a standard Kohn-Sham DFT calculation of adiabatic electronic states,

$$H|\psi_i\rangle = \epsilon_i|\psi_i\rangle. \tag{2}$$

5

Here, the states are represented by expansion coefficients in an atomic-orbital basis set

$$|\psi_i\rangle = \sum_j c_{ij}|\phi_j\rangle, \tag{3}$$

which could be obtained by projection on localized orbitals in plane-wave codes. As in most diabatization methods for electron transfer, the system is divided in electron donor (D) and acceptor regions (A). As the basis functions ϕ_j are assumed to be localized on atomic nuclei, they are assigned to donor and acceptor regions accordingly. In addition, the basis functions are orthogonalized according to the Löwdin symmetric procedure.[61,62] This leads to a block Hamiltonian representation in the orthonormal basis,

$$\tilde{H} = S^{-1/2} \cdot H \cdot S^{-1/2} = \begin{bmatrix} \tilde{H}_{DD} & \tilde{H}_{DA} \\ \tilde{H}_{AD} & \tilde{H}_{AA} \end{bmatrix} \tag{4}$$

with donor / acceptor sub-Hamiltonian blocks on the diagonal while the off-diagonal blocks describe their interaction. The desired diabatic charge transfer states are obtained by unitary transformation diagonalizing the $\tilde{H}_{\alpha\alpha}$ (α = D, A) blocks

$$\bar{H}_{\alpha\alpha} = U_\alpha^\dagger \cdot \tilde{H}_{\alpha\alpha} \cdot U_\alpha, \tag{5}$$

and the unitary matrices are used for corresponding transformation of the off-diagonal blocks,

$$\bar{H}_{\alpha\beta} = U_\alpha^\dagger \cdot \tilde{H}_{\alpha\beta} \cdot U_\beta. \tag{6}$$

The system Hamiltonian is thus transformed into the following form

$$\bar{H} = \begin{bmatrix} \bar{H}_{DD} & \bar{H}_{DA} \\ \bar{H}_{AD} & \bar{H}_{AA} \end{bmatrix} = \begin{bmatrix} \epsilon_{D,1} & \cdots & 0 & & & \\ \vdots & \ddots & \vdots & & \bar{H}_{DA} & \\ 0 & \cdots & \epsilon_{D,N} & & & \\ & & & \epsilon_{A,1} & \cdots & 0 \\ & \bar{H}_{AD} & & \vdots & \ddots & \vdots \\ & & & 0 & \cdots & \epsilon_{A,M} \end{bmatrix}. \tag{7}$$

where $\epsilon_{\alpha,i}$ are one-electron energies of the diabatic states of donor and acceptor, respectively, and the off-diagonal $\bar{H}_{\alpha\beta}$ blocks contains electronic coupling elements between the corresponding

diabatic states. Hence, by construction the orbitals coupled are strongly localized in the respective donor or acceptor regions and they may have only small tails in the acceptor or donor regions due to orthogonalization. This procedure leaves the original KS orbitals that were localized in either donor or acceptor region virtually unchanged, but leads to localization of KS orbitals that were spread over both regions.

III.   Computational Details

The POD scheme was implemented as a new module in a developer's version of the CP2K software package.[55] Cluster calculations for inter-atom ET (He_2^+, Zn_2^+), intermolecular ET (HAB11 database), intramolecular ET (Q-TTF-Q$^-$) and interfacial ET (coumarine adsorbed on TiO_2 nanoparticle) were done using a supercell approach, treating long-range interactions according to Martyna and Tuckerman.[63] The cell size was carefully chosen in these cases to be large enough not to have any system charge density on the boundaries. Calculations for ET in MgO and across extended TiO_2 and Au(111) surfaces were treated under periodic boundary conditions (PBC). Core electrons of all atoms were described by GTH atomic pseudopotentials[64] in all systems except for the helium dimer where all electrons where treated explicitly. While the Ahlrichs-def-QZVP basis set for used for helium calculations, DZ and TZ type of basis sets with polarization functions from CP2K database, compatible with GTH pseudopotentials, were applied in other systems. As for the DFT functionals, we compared the pure-GGA functional BLYP,[65,66] the hybrid functionals B3LYP[65-68] (20% HFX) and PBE0[69-71] (25% HFX), and PBE[69] with 50% HFX. The latter functional is denoted PBE50 throughout this article. In general, exact exchange helps to localize charge density and increases the band gap of solid-state materials, however, the optimal fraction of HFX is system dependent.

The limited-memory BFGS algorithm[72] as implemented in CP2K was used for geometry optimization and the structures were considered to be in total-energy minimum when the atomic forces were smaller than 10^{-4} a.u. The wavefunction was then optimized on the minimized structures with tight convergence criteria 10^{-7} a.u. before the POD method was applied. Fermi-Dirac distribution smearing with electronic temperature 298.15 K was used in metal surface calculations to maintain fractional occupation of states near the Fermi energy. The molecular orbitals were visualized by VMD[73] from their grid-calculated values.

The decay parameter β was obtained by logarithmic least-square fitting of calculated distance-dependent $|H_{ab}|$ values to exponential $Ae^{-\beta d/2}$ function. Fitting of the linearized logarithmic form rather than direct non-linear exponential fit was chosen to better capture the long-range decay of the coupling elements. For comparison with reference values, mean unsigned error (MUE, $\sum_n |y_{calc} - y_{ref}|/n$), maximum unsigned error (MAX, $\max|y_{calc} - y_{ref}|$), mean relative signed error (MRSE, $\sum_n (y_{calc} - y_{ref})/ny_{ref}$) and mean relative unsigned error (MRUE, $\sum_n |y_{calc} - y_{ref}|/ny_{ref}$) were evaluated where appropriate.

IV.   Results and Discussion

IV.1. Performance against ab-initio benchmarks

He$_2^+$ dimer

First, we investigated the positively charged helium dimer (He$_2^+$) as one of the minimal systems on which ET can be demonstrated. This system contains three electrons only, forming an open-shell doublet electronic state, and the self-exchange of the electron hole between the two atoms is expected. The diabatic charge states representing the initial and the final state of the process are assumed to be localized on the first and second atom, respectively. The small number of electrons

allows application of accurate high-level ab initio methods such as full configuration interaction (FCI). This calculation was performed by Pieniazek *et al.*[74] who published FCI/aug-cc-pV5Z value of H_{ab} obtained by formalism of generalized Mulliken-Hush (GMH) theory[26,27] at different distances of the helium atoms. We refer to these values, which were reproduced by Kubas[44] using CASSCF/MRCI+Q approach, as a reference for our calculations. As for DFT-based methods, Oberhofer[39] demonstrated excellent agreement of both CDFT and FODFT with FCI values for this minimal charge-transfer system.

As was shown previously for CDFT calculations, the H_{ab} values are rather sensitive to fraction of Hartree-Fock exchange (HFX) in the applied DFT functional.[39,44] Therefore, we compared popular functionals with different fraction of HFX, namely BLYP, B3LYP, PBE, PBE0 and PBE50. The calculated values of H_{ab} at four different He-He distances, obtained in Ahlrichs-def-QZVP basis set, are collected in Table 1. At first glance, one can notice that the increasing fraction of HFX in the applied functional leads to better agreement with the FCI reference. While the BLYP functional provides rather poor values with a mean unsigned error (MUE) of 21.8 meV, excellent agreement with the accurate reference numbers was obtained with PBE50 where MUE was reduced to 2.1 meV over the full distance range 2.5 – 5.0 Å.

The trend of increasing $|H_{ab}|$ values with larger fraction of HFX in the functional is opposite than in CDFT, which overestimates the coupling values in pure GGA and addition of HFX leads to decrease in electronic coupling. This is the consequence of different construction of the diabatic states in the two methods. In CDFT, where diabatic states are constructed directly (see Supporting Information for details), the increasing fraction of HFX helps to remove the spurious delocalization of the redox active frontier orbitals over donor and accept as seen with GGA functionals, leading to smaller electronic couplings. On the contrary, the POD approach is based

on the usual adiabatic states delocalized over donor and acceptor sites. Addition of exact exchange leads to well-known charge density increase between the atoms in the bond region, and improves the asymptotic behavior further from the molecule (see Fig. S1 in Supporting Information for comparison of PBE and PBE50 charge density profile along the principal axis of the molecule). The charge density obtained with HFX decays somewhat slower than in GGA. Therefore the PBE50 frontier HOMO / LUMO orbitals are more expanded than in PBE as can be seen in Fig 1 where their 0.001 e/Å^3 contours are shown. As the diabatic states are formed by projection of the adiabatic states, they expand in a similar manner with increasing HFX resulting in larger electronic couplings. In accord with these observations, the increase in HFX results in smaller exponential decay constants, β. In other words, the electronic coupling decay is less rapid with larger fraction of HFX in the DFT functional.

Zn_2^+ dimer

While the minimal helium dimer model was calculated at all-electron level, DFT calculations of more complex systems are typically realized using pseudopotentials to reduce the computational cost and avoid relativistic treatment of affecting core electrons in heavy atoms. To demonstrate the pseudopotential calculation on a simple and small model we explored the coupling values in Zn_2^+ for which the accurate CASSCF(3,8) and CASSCF(3,8)/MRCI+Q values of H_{ab} were published.[44] Using the analytic GTH pseudopotential for 18 core electrons[64] and optimized short-range DZV basis set available in the CP2K software package and PBE50 functional, we obtained reasonably good decay parameters of 2.24 Å^{-1} compared to 2.42 - 2.46 Å^{-1} at the CASSCF(3,8)/aug-cc-pVTZ level of theory.[44] However, absolute values of the $|H_{ab}|$ coupling elements are considerably underestimated as can be seen in Table 2. Therefore, we reoptimized the basis set for this system (see Table S4 of Supporting Information), which led to larger

coupling values and improved the decay parameter to 2.47 Å^{-1}, which is now in excellent agreement with CASSCF. The dramatic effect of the basis on accuracy in this case is not surprising because the DZV basis available in the CP2K database is short-range, which means that it was optimized for molecular calculations within periodic-boundary conditions, where rapid decay of charge density is desirable to eliminate artificial interactions of a molecule with its nearest images. However, quantitative H_{ab} calculation for intermolecular charge transfer at medium and large distance requires good description of the wavefunction tail, for which more extended basis sets including diffuse functions are appropriate.

Intermolecular ET in organic dimers

Next, we benchmarked the POD method against the HAB11 database[44] of small cationic organic-molecule homo dimers. The molecules contain single, double and triple bonds (ethylene, acetylene, cyclopropene), they have different type of aromaticity (antiaromatic cyclobutadiene, nonaromatic cyclopentadiene, aromatic benzene) and different heteroatoms (oxygen in furane, nitrogen in pyrrole and imidazole, sulfur in thiophene). All the homo-dimers have single positive charge and doublet spin multiplicity. Accurate MRCI+Q and NEVPT2 ab initio reference values are available for distances of 3.5, 4.0, 4.5 and 5.0 Å and both CDFT and FODFT methods were already benchmarked against them[44] using the PBE functional. While FODFT was found to systematically underestimate the coupling values due to neglect of interaction between the monomers, CDFT overestimated $|H_{ab}|$ at GGA level and performance improved with added fraction of HFX, following a trend similar to the one described for the helium dimer. A fraction of 50 % of HFX was found to give optimal performance of CDFT on the HAB11 database.

Values calculated with the POD method for PBE, PBE0 and PBE50 functional, GTH pseudopotentials and TZV2P basis set are collected in Table 3. In general, the coupling values

follow the same trends that we observed in He_2^+. While the absolute values are considerably underestimated in GGA and converge to reference values as the HFX fraction is increased, the decay parameters are overestimated for GGA and then decreases with addition of exact exchange (see Table S5 in Supporting Information where the statistical errors are evaluated). These effects are a direct consequence of self-interaction error causing artificial delocalization of charge density in GGA, which is corrected by HFX as we discussed above. As in the case of CDFT, we found PBE50 as the optimal choice for calculating the absolute $|H_{ab}|$ values. The same conclusion is valid for the decay parameter, although the PBE0 and PBE50 results exhibit similar mean errors. Overall, we can conclude that the POD method as implemented in CP2K is able to describe electronic coupling for organic inter-molecular charge transfer at a quantitative level, and the results are comparable with the CDFT and FODFT values.

Intramolecular ET in Q-TTF-Q⁻

Although no ab-initio reference data are available for this system, we include it here as it has been investigated before at the DFT level. A number of groups have carried out CDFT coupling calculations on this molecule and reported consistent results, Wu and Van Voorhis[37] 133.3 meV (B3LYP), Oberhofer and Blumberger[39] 304.8 meV (BLYP) and 103.4 meV (B3LYP), and Holmberg and Laasonen[75] 459.9 meV (PBE) and 98.0 meV (PBE0). Renz and Kaupp reported a value of 119.3 meV as obtained from the adiabatic energy splitting at TDDFT/BLYP35 functional level.[76]

The POD method applied to the Q-TTF-Q⁻ anion, with donor / acceptor regions defined as left / right half of the molecule, yielded coupling values of 19.8 meV for BLYP/TZVP and 20.4 meV for TZV2P basis set. The coupling magnitude increased to 24.4 meV at B3LYP/TZVP and to 37.6 meV at HF/TZVP level of theory. The values obtained were robust against further expansion of

the basis set with diffuse functions, reduction of the D-A regions to the quinone moeities of the molecule and re-optimization of the (symmetric) transition state structure with different DFT functionals. Although the diabatic states are localized on the quinones (see Fig. 2), in qualitative agreement with the CDFT states found in Ref. 39, POD coupling values are considerably lower than in CDFT and in better agreement with experimental estimates[77] (~ 20 meV, obtained from the experimental rate constant and activation free energy in a ethyl acetate/*terc*-butanol solvent mixture ($1.3 \cdot 10^8$ s^{-1} and 6.4 kcal/mol, respectively); note that the experimental estimate was not correctly cited in Ref. 39). The lower coupling value obtained with POD is most likely related to the inherently different construction of the Hamiltonian coupling the diabatic states in this method compared to CDFT.

IV.2. Interfacial ET

Coumarine 343 on TiO$_2$

In the following we investigate electronic coupling for interfacial ET, specifically for electron injection from the dye-molecule coumarine 343 (C343) to the conduction band of an anatase TiO$_2$ nanoparticle. This system has been of interest for dye-sensitized solar cell (DSSC) applications and was previously studied by Kondov *et al.*[51] At first, we built a C343-(TiO$_2$)$_{24}$(H$_2$O)$_{30}$ cluster model as described in Ref. 51, where unsaturated vacancies of the titania surface were capped by water molecules. The whole model was pre-optimized with the Gaussian 09 program[78] using the B3LYP functional with SDD pseudopotentials and a corresponding pseudobasis[79] for titanium atoms and a minimal Pople's STO-3G basis set[80] for the rest of the system. Then, the geometry was fully optimized in CP2K using the PBE functional, GTH pseudopotentials and DZVP basis

set. The PBE functional was chosen to ensure consistent comparison with the extended-surface calculations discussed further below.

The final structure with the donor state localized on the coumarine molecule and a representative vacant state from the conduction band of titania are shown in Fig. 2. As can be seen from the energy-level diagram plotted in Fig. 3, the donor state is the LUMO of the molecule located about 2.1 eV above the system Fermi level and the electron can be injected into one of the nearby empty states near the TiO_2 conduction-band minimum.

We find that the nanoparticle structure is affected by significant surface distortions that are inevitably present in the cluster model. To eliminate this effect, we created, for comparison, an analogous model with a anatase (101) slab simulating the extended surface by application of periodic boundary conditions (PBC). The structure is shown in Fig. 2. As can be seem from Fig. 3, the electronic states are more closely packed in the valence / conduction bands. The calculated band gap of 2.1 eV is consistent with published bulk values for PBE, 1.94 – 2.16 eV[81-83] and underestimated comparing to the experimental value for bulk anatase (3.2 – 3.4 eV),[84,85] as expected for GGA functionals. As in the cluster model, the donor state is the first molecular state above the Fermi energy ideally positioned for electron injection into the dense conduction band of titania.

The coupling elements between the donor state and the TiO_2 conduction band are plotted in Fig. 4. Both cluster and periodic models predict 20 – 30 meV strong coupling elements to conduction band states of similar energy and values of up to about 100 meV for coupling to higher energy conduction band states. The distribution of couplings for the cluster model is in good agreement with the one reported by Kondov *et al*.[51] Small deviations are likely due to different geometries and different functional/basis set used. While the calculations in Ref. 51 were carried

out using the B3LYP functional and SV(P) basis set, we employed PBE, DZVP basis set and GTH pseudopotentials.

We would like to note that the issue of energy level alignment in (uncorrected) density functional theory will also affect the calculation of electronic coupling matrix elements. Here we use PBE in a proof-of-concept application to allow for validation of our POD implementation by comparison with DFT calculations reported previously in the literature. More elaborate electronic structure methods, as e.g. GW or the more cost effective DFT+Σ approach,[86-88] which adds a self-energy correction to the DFT electronic level alignment, are likely to improve the accuracy of the coupling matrix element calculation for semiconducting and metallic interfaces. Overall, the results obtained here for electron injection into titania further validate our implementation and demonstrate applicability of the POD method to semiconductor surface charge-transfer phenomena that have great importance in many technological applications.

Alkanethiolate on Au(111)

Electron injection from an organic molecule to the gold (111) surface was investigated as an example for heterogeneous electron transfer across a molecule / metal interface. Specifically, we studied a series of nitrile substituted alkanethiolates with increasing chain length n, $HCS(CH_2)_nCN$. The molecules chemically adsorb on the Au surface via the sulphur anchor. Kao et al.[89] measured electron injection times of 14 fs, 35 fs and 100 fs for $n = 2$, 3 and 4, respectively, by resonant Auger electron spectroscopy. Later, Prucker et al.[54] calculated electronic couplings between the nearly degenerate π_1^*, π_2^* states localized on the terminal CN group of the alkanethiolates and the vacant gold-surface states. They confirmed, by computing the injection times from time-dependent state populations, that the charge transfer depends on the molecular

chain lengths and it increases from a few femtoseconds ($n = 2$) to picoseconds ($n = 8$). The two π^* states were shown to have different orientations which affect the coupling and consequently the electron-transfer rates and the injection times.[90]

We optimized structures of the $HCS(CH_2)_nCN$ molecules ($n = 2$ to 8) on Au(111), the latter consisting of 5 layers of atoms. The gold slab was cut from a cubic closed-packed crystal structure with lattice constant 4.066 Å, which was found optimal (in terms of bulk total energy variations with cell size) for the applied PBE functional with GTH pseudopotentials for 68 core electrons and corresponding TZ basis set. The positions of the atoms in the two bottom layers were constrained to the bulk geometry while the upper three layers and the molecule were free to relax during the optimization. The electronic coupling elements were then evaluated on these structures with the POD approach with the system partitioned in two blocks – the molecule and the gold slab.

Final structures including isosurfaces of the π_1^* orbitals are shown in Fig. 5 while the π_2^* states can be seen in Fig. S4. The orbitals are located on the CN groups of the molecules and since π_1^* and π_2^* are eigenvectors of the same Hamiltonian block they are mutually orthogonal and have different orientation with respect to the surface (compare Fig. 5 and Fig. S4 in Supporting Information). Energetically, the states are quasi-degenerate, located 4.0 – 4.7 eV above the Fermi energy, as can be seen in Fig. S5 of Supporting Information where the state energies are plotted. The two π^* states are clearly LUMO+1 and LUMO+2 of the molecule while the frontier HOMO / LUMO orbitals are localized on the anchoring sulfur atom. While the π_2^* state is strictly localized on the terminal $-CH_2CN$ part of the molecule, the π_1^* state tends to be more delocalized over the alkyl chain, which affects the electronic coupling to vacant surface states.[54,90]

The values of the coupling elements $|H_{ab}|$ to the gold states from the π_1^* donor state are plotted

in Fig. 6 and from the π_2^* states in Fig. S6. The decreasing trend with increasing chain length is

clearly visible in both cases (note different energy scales on the vertical axes of the plots). While

the strongest coupling elements reach 60 – 70 meV in the shortest $HCSCH_2CN$ molecule, they

drop by a factor of about 10 to 4 – 6 meV in case of the longest $HCS(CH_2)_7CN$ chain. In general,

the magnitudes of couplings obtained for the π_2^* state are lower than those for the π_1^* state, which

is a consequence of increased localization and different orientation of the π_2^* state. We find that

the distance decay of electronic coupling is well described by an exponential with a decay

constant $\beta = 1.01$ $(\pi_{1,}^*)$ and 1.34 (π_2^*) per CH_2 unit, in good agreement with Ref. 54 (0.94 for π_2^*)

and with experimental estimates obtained from the chain-length dependence of injection times,

0.93.[89] We note that the values obtained here from calculations under periodic boundary

conditions are in remarkably good agreement with the values obtained from finite cluster

calculations as reported by Prucker *et al.*[54]

IV.3. ET in bulk oxide

When evaluating the performance of the POD method on a total of 7 ET systems, we have

encountered one system where agreement with previously published results was less good, the

hole transfer between F center defects (oxygen vacancies) in MgO, that is $F_a^0 + F_b^+ \rightarrow F_a^+ + F_b^0$.

This charge-transfer process was investigated by McKenna and Blumberger[59,60] who argued that

for the coupling calculations a functional should be used that reproduces the experimental band

gap of MgO (in this case, PBE0 7.2 eV[60] vs. experimental 7.2 – 7.8 eV.[91-95] Our calculations on

bulk MgO performed with CP2K reproduced this value using the same functional, GTH

pseudopotentials and DZVP basis set. As one can appreciate, the definition of the donor / acceptor

regions is somewhat arbitrary in bulk materials like MgO. In previous work[60] it was found that the

spin density corresponding to the electron hole is localized in the vicinity of the oxygen vacancies and its shape is a superposition of an s-like function centered at the vacant site and p-functions of the nearest six oxygen atoms. Therefore, the donor region was defined as the "left" half of the supercell containing the neutral oxygen vacancy and the acceptor as the "right" half of the supercell containing the positively charged vacancy (see visualization of regions in Fig. S8). As there are an odd number of layers between the two vacancies, the middle MgO layer is at the same distance from either of the two vacancies. Hence, this layer was not included in either regions.

Using this D/A definition, we obtained considerably lower coupling values with the POD method than in CDFT, see Table 4. The largest discrepancy was found with vacancies oriented along the (100) direction, at the largest distance (12.8 Å). This suggests that the spin density between the two centers decays more rapidly in POD than in CDFT. However, the coupling values could be also affected by the size of the D-A regions used for diabatizing the projection. Indeed, when we included the middle layer in the donor region, the coupling values increased significantly in case of the (100) and (110) models, but the charge state becomes too delocalized in the (111) structure leading to artificially high couplings in this case. We conclude that for ET within bulk solids, POD couplings have to be interpreted with care as they are likely to be sensitive to the precise definition of donor and acceptor regions.

Conclusions

We implemented the projection-operator diabatization (POD) method for electronic coupling calculation in the CP2K program package. By investigation of charge transfer in cationic dimers of atoms and small organic molecules, we showed that the POD method is comparable in accuracy to the CDFT method providing that the adiabatic KS orbitals, used for construction of

the localized orbitals, are calculated with an appropriate functional and basis set. In particular, the fraction of exact exchange was found to have a major effect on the correct shape of the adiabatic states and consequently, on the accuracy of the coupling elements, which is typical for application of DFT on molecular systems.

The method could be applied to complex periodic systems, specifically to ET at molecule / metal and semiconductor interfaces where the division of the system in donor / acceptor regions arise naturally. We demonstrated electron injection from the discrete donor states of an organic molecule to the delocalized band states of the semiconductor TiO_2 for both cluster model and periodic surface model. Moreover, electron transfer to metallic surfaces could be investigated straightforwardly, as demonstrated in this work for charge transfer from an adsorbed organic molecule to Au(111). In further applications to interfacial ET problems, the POD method should be used in combination with DFT approaches that reproduce the energy level alignment of the molecular states with respect to the metal / semiconductor. This issue and its effect on electronic coupling calculation will be investigated in future work.

Acknowledgements

Supporting Information

Brief summary of CDFT and FODFT theory, comparison of charged and neutral model of He_2 dimer, coupling basis-set dependence in He_2 models, specification of reoptimized basis set for Zn_2^+, statistical error for coupling and decay parameter values benchmarked on HAB11 database, PDOS comparison of TiO_2 / C343 obtained in cluster and surface model, energy-level diagrams of Au(111) / $HCS(CH_2)_nCN$ interfaces, localization of π_2^* molecular orbitals and electronic couplings between the π_2^* states and empty states of the gold surface, estimation of Q-TTF-Q^- coupling from experimental data, visualization of MOs and D-A regions in bulk MgO models, XYZ structure files with TiO_2 / C343 and Au(111) / $HCS(CH_2)_nCN$ model coordinates.

References

(1)   Mitchell, P. Coupling of Photosphorylation to Electron and Hydrogen Transfer by a Chem-Osmotic Type of Mechanism. *Nature* **1961**, *191*, 144-148.

(2)   Fleming, G. R.; Martin, J.-L. Breton, J. Rates of Primary Electron Transfer in Photosynthetic Reaction Centers and Their Mechanistic Implications. *Nature* **1988**, *333*, 190-192.

(3)   Ferreira, K. N.; Iverson, T. N.; Maghlahoui, K.; Barber, J.; Iwata, S. Architecture of the Photosynthetic Oxygen-Evolving Center. *Science* **2004**, *303*, 1831-1838.

(4)   Barber, J. Photosynthetic Energy Conversion: Natural and Artificial. *Chem. Soc. Rev.* **2009**, *38*, 185-196.

(5)   Abrahams, J. P.; Leslie, A. G.; Lutter, R.; Walker, J. E. Structure at 2.8 A Resolution of F1-ATPase from Bovine Heart Mitochondria. *Nature* **1977**, *266*, 271-273.

(6)   Cecchini, G. Function and Structure of Complex II of the Respiratory Chain. *Annu. Rev. Biochem.* **2003**, *72*, 77-109.

(7)   Crofts, A. R. The Cytochrome bc1 Complex: Function in the Context of Structure. *Annu. Rev. Physiol.* **2004**, *66*, 689-733.

(8)   Hirst, J. Mitochondrial Complex I. *Annu. Rev. Biochem.* **2013**, *82*, 551-575.

(9)   Sazanov, L. A. A Giant Molecular Proton Pump: Structure and Mechanism of Respiratory Complex I. *Nat. Rev. Mol. Cell Biol.* **2015**, *16*, 375-388.

(10) Adman, E. T. Copper Protein Structures. *Adv. Protein Chem.* **1991**, *42*, 145-197.

(11) Armstrong, F. A.; Heering, H. A.; Hirst, J. Reactions of Complex Metalloproteins Studied by Protein-Film Voltammetry. *Chem. Soc. Rev.* **1997**, *26*, 169-179.

(12) Lukin, J. A.; Ho, C. The Structure-Function Relationship of Hemoglobin in Solution at Atomic Resolution. *Chem. Rev.* **2004**, *104*, 1219-1230.

(13) Vincent, K. A.; Parkin, A. Armstrong, F. A. Investigating and Exploiting the Electrocatalytic Properties of Hydrogenases. *Chem. Rev.* **2007**, *107*, 4366-4413.

(14) Liu, J.; Chakraborty, S.; Hosseinzadeh, P.; Yu, Y.; Tian, S.; Petrik, L.; Bhagi, A.; Lu, Y. Metalloproteins Containing Cytochrome, Iron-Sulfur, or Copper Redox Centers. *Chem. Rev.* **2014**, *114*, 4366-4469.

(15) Winkler, J. R.; Gray, H. B. Electron Flow through Metalloproteins. *Chem. Rev.* **2014**, 3369-3380.

(16) Gong, J.; Liang, J.; Sumathy, K. Review on Dye-Sensitized Solar Cells (DSSCs): Fundamental Concepts and Novel Materials. *Renew. Sustainable Energy Rev.* **2012**, *16*, 5848-5860

(17) Yan, J.; Saunders, B. R. Third-Generation Solar Cells: A Review and Comparison of Polymer/Fullerene, Hybrid Polymer and Perovskite Solar Cells. *RSC Adv.* **2014**, *4*, 43286-43314.

(18) Goodenough, J. B.; Park, K. S. The Li-Ion Rechargeable Battery: A Perspective. *J. Am. Chem. Soc.* **2013**, *135*, 1167-1176.

(19) Choi, J. W.; Aurbach, D. Promise and Reality of Post-Lithium-Ion Batteries with High Energy Densitites. *Nature Rev. Mater.* **2016**, *1*, 1-16.

(20) Gray, H. B.; Winkler, J. R. Long-Range Electron Transfer. *Proc. Natl. Acad. Sci. U.S.A.* **2005**, *102*, 3534-3539.

(21) Kastlunger, G.; Stadler, R. Density Functional Theory Based Calculations of the Transfer Integral in a Redox-Active Single-Molecule Junction. *Phys. Rev. B* **2014**, *89*, 115412.

(22) Marcus, R. A. On the Theory of Oxidation-Reduction Reactions Involving Electron Transfer. I. *J. Chem. Phys.* **1956**, *24*, 966-978.

(23) Marcus, R. A. Electrostatic Free Energy and Other Properties of States Having Nonequilibrium Polarization. I. *J. Chem. Phys.* **1956**, *24*, 979-989.

(24) Pacher, T.; Cederbaum, L. S.; Koppel, H. Approximately Diabatic States from Block Diagonalization of the Electronic Hamiltonian. *J. Chem. Phys.* **1988**, *89*, 7367-7381.

(25) Domcke, W.; Woywod, C. Direct Construction of Diabatic States in the CASSCF Approach. Application to the Conical Intersection of the $^1A_2$ and $^1B_1$ Excited States of Ozone. *Chem. Phys. Lett.* **1993**, *216*, 362-368.

(26) Cave, R. J.; Newton, M. D. Generalization of the Mulliken-Hush Treatment for the Calculation of Electron Transfer Matrix Elements. *Chem. Phys. Lett.* **1996**, *249*, 15-19.

(27) Cave, R. J.; Newton, M. D. Calculation of Electronic Coupling Matrix Elements for Ground and Excited State Electron Transfer Reactions: Comparison of the Generalized Mulliken-Hush and Block Diagonalization Methods. *J. Chem. Phys.* **1997**, *106*, 9213-9226.

(28) Voityuk, A. A.; Rosch, N. Fragment Charge Difference Method for Estimating Donor-Acceptor Electronic Coupling: Application to DNA π-stacks. *J. Chem. Phys.* **2002**, *117*, 5607-5616.

(29) Hsu, C.-P.; You, Z.-Q.; Chen, H.-C. Characterization of the Short-Range Couplings in Excitation Energy Transfer. *J. Phys. Chem. C* **2008**, *112*, 1204-1212.

(30) Migliore, A.; Corni, S.; Di Felice, R.; Molinari, E. First-Principles Density-Functional Theory Calculations of Electron-Transfer Rates in Azurin Dimers. *J. Chem. Phys.* **2006**, *124*, 064501.

(31) Migliore, A.; Sit, P. H.-L.; Klein, M. L. Evaluation of Electronic Coupling in Transition-Metal Systems Using DFT: Application to the Hexa-Aquo Ferric-Ferrous Redox Couple. *J. Chem. Theory Comput.* **2009**, *5*, 307-323.

(32) Senthilkumar, K.; Grozema, F. C.; Bickelhaupt, F. M.; Siebbeles, L. D. A. Charge Transport in Columnar Stacked Triphenylenes: Effects of Conformational Fluctuations on Charge Transfer Integrals and Site Energies. *J. Chem. Phys.* **2003**, *119*, 9809-9817.

(33) Oberhofer, H.; Blumberger, J. Insight into the Mechanism of the Ru^{2+}-Ru^{3+} Electron Self-Exchange Reaction from Quantitative Rate Calculations. *Angew. Chem. Int. Ed.* **2010**, *49*, 3631-3634.

(34) Oberhofer, H.; Blumberger, J. Revisiting Electronic Couplings and Incoherent Hopping Models for Electron Transport in Crystalline C_{60} at Ambient Temperatures. *Phys. Chem. Chem. Phys.* **2012**, *14*, 13846-13852.

(35) Gajdos, F.; Oberhofer, H.; Dupuis, M.; Blumberger, J. Inapplicability of Electron Hopping Models for the Organic Semiconductor Phenyl-C61-butyric Acid Methyl Ester (PCBM). *J. Phys. Chem. Lett.* **2013**, *4*, 1012-1017.

(36) Gajdos, F.; Oberhofer, H.; Dupuis, M.; Blumberger, J. Correction to "Inapplicability of Electron Hopping Models for the Organic Semiconductor Phenyl-C61-butyric Acid Methyl Ester (PCBM)". *J. Phys. Chem. Lett.* **2014**, *5*, 2765-2766.

(37) Wu, Q.; Van Voorhis, T. Extracting Electron Transfer Coupling Elements from Constrained Density Functional Theory. *J. Chem. Phys.* **2006**, *125*, 164105.

(38) Wu, Q.; Van Voorhis, T. Direct Calculation of Electron Transfer Parameters through Constrained Density Functional Theory. *J. Phys. Chem. A* **2006**, *110*, 9212-9218.

(39) Oberhofer, H.; Blumberger, J. Electronic Coupling Matrix Elements from Charge Constrained Density Functional Theory Calculations Using a Plane Wave Basis Set. *J. Chem. Phys.* **2010**, *133*, 244105

(40) Gillet, N.; Berstis, L.; Wu, X.; Gajdos, F.; Heck, A.; de la Lande, A.; Blumberger, J.; Elstner, M. Electronic Coupling Calculations for Bridge-Mediated Charge Transfer Using Constrained Density Functional Theory (CDFT) and Effective Hamiltonian Approaches at the Density Functional Theory (DFT) and Fragment-Orbital Density Functional Tight Binding (FODFTB) Level. *J. Chem. Theory Comput.* **2016**, *12*, 4793-4805.

(41) Gajdos, F.; Valner, S.; Hoffmann, F.; Spencer, J.; Breuer, M.; Kubas, A.; Dupuis, M.; Blumberger, J. Ultrafast Estimation of Electronic Couplings for Electron Transfer between π-Conjugated Organic Molecules. *J. Chem. Theory Comput.* **2014**, *10*, 4653-4660.

(42) Zhang, Y.; Yang, W. A Challenge for Density Functionals: Self-Interaction Error Increases for Systems with Noninteger Number of Electrons. *J. Chem. Phys.* **1998**, *109*, 2604-2608.

(43) Cohen, A. J.; Mori-Sanchez, P.; Yang, W. Insights into Current Limitations of Density Functional Theory. *Science* **2008**, *321*, 792-794.

(44) Kubas, A.; Hoffmann, F.; Heck, A.; Oberhofer, H.; Elstner, M.; Blumberger, J. Electronic Couplings for Molecular Charge Transfer: Benchmarking CDFT, FODFT, and FODFTB Against High-Level *Ab Initio* Calculations. *J. Chem. Phys.* **2014**, *140*, 104105.

(45) Kubas, A.; Gajdos, F.; Heck, A.; Oberhofer, H.; Elstner, M.; Blumberger, J. Electronic Couplings for Molecular Charge Transfer: Benchmarking CDFT, FODFT, and FODFTB Against High-Level *Ab Initio* Calculations. II. *Phys. Chem. Chem. Phys.* **2015**, *17*, 14342-14354.

(46) Wu, Q.; Cheng, C.-L.; Van Voorhis, T. Configuration Interaction Based on Constrained Density Functional Theory: A Multireference Method. *J. Chem. Phys.* **2007**, *127*, 164119.

(47) Marcus, R. A. On the Theory of Electron-Transfer Reactions. VI. Unified Treatment for Homogeneous and Electrode Reactions. *J. Chem. Phys.* **1965**, *43*, 679-701.

(48) Hush, N. S. Adiabatic Rate Processes at Electrodes. I. Energy-Charge Relationships. *J. Chem. Phys.* **1958**, *28*, 962-972.

(49) Chidsey, Ch. E. D. Free Energy and Temperature Dependence of Electron Transfer at the Metal-Electrolyte Interface. *Science* **1991**, *251*, 919-922.

(50) Bard, A. J.; Faulkner, L. R. *Electrochemical Methods. Fundamentals and Applications.* Second Edition. John Wiley & Sons, Inc. 2001.

(51) Kondov, I.; Cizek, M.; Benesch, C.; Wang, H.; Thoss, M. Quantum Dynamics of Photoinduced Electron-Transfer Reactions in Dye-Semiconductor Systems: First-Principles Description and Application to Coumarin 343-TiO$_2$. *J. Phys. Chem. C* **2007**, *111*, 11970-11981.

(52) Li, J.; Nilsing, M.; Kondov, I.; Wang, H.; Persson, P.; Lunell, S.; Thoss, M. Dynamical Simulations of Photoinduced Electron Transfer Reactions in Dye-Semiconductor Systems with Different Anchor Groups. *J. Phys. Chem. C* **2008**, *112*, 12326-12333.

(53) Li, J.; Kondov, I.; Wang, H.; Thoss, M. Theoretical Study of Photoinduced Electron-Transfer Processes in the Dye-Semiconductor System Alizarin-TiO$_2$. *J. Phys. Chem. C* **2010**, *114*, 18481-18493.

(54) Prucker, V.; Rubio-Pons, O.; Bockstedte, M.; Wang, H.; Coto, P. B.; Thoss, M. Dynamical Simulation of Electron Transfer Processes in Alkanethiolate Self-Assembled Monolayers at the Au(111) Surface. *J. Phys. Chem. C* **2013**, *117*, 25334-25342.

(55) Hutter, J.; Iannuzzi, M.; Schiffmann, F.; VandeVondele, J. CP2K: Atomistic Simulations of Condensed Matter System. *WIREs Comput. Mol. Sci.* **2014**, *4*, 15-25.

(56) Lippert, G.; Hutter, J.; Parrinello, M. A Hybrid Gaussian and Plane Wave Density Functional Scheme. *Mol. Phys.* **1997**, *92*, 477-487.

(57) Lippert G.; Hutter, J.; Parrinello, M. The Gaussian and Augmented-Plane-Wave Density Functional Method for Ab Initio Molecular Dynamics Simulations. *Theor. Chem. Acc.* **1999**, *103*, 124-140.

(58) VandeVondele, J.; Krack, M.; Mohamed, F.; Parrinello, M.; Chassaing, T.; Hutter, J. Quickstep: Fast and Accurate Density Functional Calculations Using a Mixed Gaussian and Plane Waves Approach. *Comput. Phys. Commun.* **2005**, *167*, 103-128.

(59) McKenna, K. P.; Blumberger, J. Crossover from Incoherent to Coherent Tunneling Between Defects in MgO. *Phys. Rev. B* **2012**, *86*, 245110

(60) Blumberger, J.; McKenna, K. P. Constrained Density Functional Theory Applied to Electron Tunnelling Between Defects in MgO. *Phys. Chem. Chem. Phys.* **2013**, *15*, 2184-2196.

(61) Lowdin, P.-O. On the Non-Orthogonality Problem Connected with the Use of Atomic Wave Functions in the Theory of Molecules and Crystals. *J. Chem. Phys.* **1950**, *18*, 365-375.

(62) Mayer, I. On Lowdin's Method of Symmetric Orthogonalization. *Int. J. Quant. Chem.* **2002**, *90*, 63-65.

(63) Martyna, G. J.; Tuckerman, M. E. A Reciprocal Space Based Method for Treating Long Range Interactions in Ab Initio and Force-Field-Based Calculations in Clusters. *J. Chem. Phys.* **1999**, *110*, 2810-2821.

(64) Goedecker, S.; Teter, M.; Hutter, J. Separable Dual-Space Gaussian Pseudopotentials. *Phys. Rev. B* **1996**, *54*, 1703-1710.

(65) Becke, A. D. Density-Functional Exchange-Energy Approximation with Correct Asymptotic Behavior. *Phys. Rev. A* **1988**, *38*, 3098-3100.

(66) Lee, C.; Yang, W.; Parr, R. G. Development of the Colle-Salvetti Correlation-Energy Formula into a Functional of the Electron Density. *Phys. Rev. B* **1988**, *37*, 785-789.

(67) Vosko, S. H.; Wilk, L.; Nusair, M. Accurate Spin-Dependent Electron Liquid Correlation Energies for Local Spin Density Calculations: A Critical Analysis. *Can. J. Phys.* **1980**, *58*, 1200-1211.

(68) Becke, A. D. Density-Functional Thermochemistry. III. The Role of Exact Exchange. *J. Chem. Phys.* **1993**, *98*, 5648-5652.

(69) Perdew, J. P.; Burke, K.; Ernzerhof, M. Generalized Gradient Approximation Made Simple. *Phys. Rev. Lett.* **1996**, *77*, 3865-3868.

(70) Adamo, C.; Barone, V. Towards Reliable Density Functional Methods Without Adjustable Parameters: The PBE0 Model. *J. Chem. Phys.* **1999**, *110*, 6158-6169.

(71) Ernzerhof, M.; Scuseria, G. E. Assesment of the Perdew-Burke-Ernzerhof Exchange-Correlation Functional. *J. Chem. Phys.* **1999**, *110*, 5029-5036.

(72) Byrd, R. H.; Lu, P.; Nocedal, J.; Zhu, C. A Limited Memory Algorithm for Bound Constrained Optimization. *SIAM J. Sci. Comput.* **1995**, *16*, 1190-1208.

(73) Humphrey, H.; Dalke, A.; Schulten, K. VMD – Visual Molecular Dynamics. *J. Molec. Graphics* **1996**, *14*, 33-38.

(74) Pieniazek, P. A.; Arnstein, S. A.; Bradforth, S. E.; Krylov, A. I.; Sherrill, C. D. Benchmark Full Configuration Interaction and Equation-of-Motion Coupled-Cluster Model with Single and Double Substitutions for Ionized Systems Results for Prototypical Charge Transfer Systems: Noncovalent Ionized Dimers. *J. Chem. Phys.* **2007**, *127*, 164110.

(75) Holmberg, N.; Laasonen, K. Efficient Constrained Density Functional Theory Implementation for Simulation of Condensed Phase Electron Transfer Reactions. *J. Chem. Theory. Comput.* **2017**, *13*, 587-601.

(76) Renz, M.; Kaupp, M. Predicting the Localized/Delocalized Character of Mixed-Valence Diquinone Radical Anions. Toward the Right Answer for the Right Reason. *J. Phys. Chem. A* **2012**, *116*, 10629-10637.

(77) Gautier, N.; Dumur, F.; Lloveras, V.; Vidal-Gancedo, J.; Veciana, J.; Rovira, C.; Hudhomme, P. Intramolecular Electron Transfer Mediated by a Tetrathiafulvalene Bridge in a Purely Organic Mixed-Valence System. *Angew. Chem. Int. Ed.* **2003**, *42*, 2765-2768.

(78) Gaussian 09, Revision E.01, Frisch, M. J.; Trucks, G. W.; Schlegel, H. B.; Scuseria, G. E.; Robb, M. A. *et al.* Gaussian, Inc., Wallingford CT, 2016.

(79) Andrae, D.; Haußermann, U.; Dolg, M.; Stoll, H.; Preuß, H. Energy-Adjusted Ab Initio Pseduopotentials for the Second and Third Row Transition Elements. *Theor. Chim. Acta* **1990**, *77*, 123-141.

(80) Hehre, W. J.; Steward, R. F.; Pople, J. A. Self-Consistent Molecular-Orbitals Methods. I. Use of Gaussian Expansions of Slater-Type Atomic Orbitals. *J. Chem. Phys.* **1969**, *51*, 2657-2664.

(81) Mattioli, G.; Alippi, P.; Filippone, F.; Caminiti, R.; Bonapasta, A. A. Deep versus Shallow Behavior of Intrinsic Defects in Rutile and Anatase TiO_2 Polymorphs. *J. Phys. Chem. C* **2010**, *114*, 21694-21704.

(82) Langmann, M.; Rauls, E.; Schmidt, W. G. The Electronic Structure and Optical Response of Rutile, Anatase and Brookite TiO_2. *J. Phys. Condens. Matter* **2012**, *24*, 195503.

(83) Zhu, T.; Gao, S.-P. The Stability, Electronic Structure, and Optical Property of TiO_2 Polymorphs. *J. Phys. Chem. C* **2014**, *118*, 11385-11396.

(84) Kavan, L.; Gratzel, M.; Gilbert, S. E.; Klemenz, C.; Scheel, H. J. Electrochemical and Photochemical Investigation of Single-Crystal Anatase. *J. Am. Chem. Soc.* **1996**, *118*, 6716-6723.

(85) Tang, H.; Levy, F.; Berger, H.; Schmid, P. E. Urbach Tail of Anatase TiO_2. *Phy. Rev. B* **1995**, *52*, 7771-7774.

(86) Neaton, J. B.; Hybertsen, M. S.; Louie, S. G. Renormalization of Molecular Electronic Levels at Metal-Molecule Interfaces. *Phys. Rev. Lett.* **2006**, *97*, 216405.

(87) Garcia-Lastra, J. M.; Rostgaard, C.; Rubio, A.; Thygesen, K. S. Polarization-Induced Renormalization of Molecular Levels at Metallic and Semiconducting Surfaces. *Phys. Rev. B* **2009**, *80*, 245427.

(88) Chen, Y.; Tamblyn, I.; Quek, S. Y. Energy Level Alignment at Hybridized Organic-Metal Interfaces: The Role of Many-Electron Effects. *J. Phys. Chem. C* **2017**, *121*, 13125-13134.

(89) Kao, P.; Neppl, S.; Feulner, P.; Allara, D. L.; Zharnikov, M. Charge Transfer Time in Alkanethiolate Self-Assembled Monolayers via Resonant Auger Electron Spectroscopy. *J. Phys. Chem. C* **2010**, *114*, 13766-13773.

(90) Blobner, F.; Coto, P. B.; Allegretti, F.; Bockstedte, M.; Rubio-Pons, O.; Wang, H.; Allara, D. L.; Zharnikov, M.; Thoss, M.; Feulner, P. Orbital-Symmetry-Dependent Electron Transfer through Molecules Assembled on Metal Substrates. *J. Phys. Chem. Lett.* **2012**, *3*, 436-440.

(91) Roessler, D. M.; Walker, W. C. Electronic Spectrum and Ultraviolet Optical Properties of Crystalline MgO. *Phys. Rev.* **1967**, *159*, 733.

(92) Whited, R. C.; Flaten, C. J.; Walker, W. C. Exciton Thermoreflectance of MgO and CaO. *Solid. State. Commun.* **1973**, *13*, 1903-1905.

(93) Lindner, T.; Sauer, H.; Engel, W.; Kambe, K. Near-Edge Structure in Electron-Energy-Loss Spectra of MgO. *Phys. Rev. B* **1986**, *33*, 22.

(94) Rafferty, B.; Brown, L. M. Direct and Indirect Transitions in the Region of the Band Gap Using Electron-Energy-Loss Spectroscopy. *Phys. Rev. B* **1998**, *58*, 10326.

(95) Schamm, S.; Zanchi, G.; Study of the Dielectric Properties Near the Band Gap by VEELS: Gap Measurement in Bulk Materials. *Ultramictroscopy* **2003**, *96*, 559-564.

Tables and Figures

Table 1: Electronic coupling $|H_{ab}|$ values [meV] for He_2^+ dimer electron self-exchange and the decay rate parameter β [Å^{-1}] fitted to $|H_{ab}| = Ae^{-\beta d/2}$ function. The values are for coupling between the block-diagonalized minority spin HOMO and LUMO orbitals on donor and acceptor atoms, respectively. The total charge of the system was +1.

d [Å]	BLYP	B3LYP	PBE0	PBE50	FCI[a]
2.5	134.26	156.32	158.70	189.51	195.93
3.0	38.18	47.17	48.48	62.04	60.81
4.0	2.28	3.95	4.25	6.23	5.52
5.0	0.21	0.32	0.33	0.54	0.44
β [Å^{-1}]	5.17	4.96	4.93	4.69	4.88

[a] Reference 39

Table 2: Electronic coupling $|H_{ab}|$ values [meV] for Zn_2^+ dimer self-exchange and the decay rate parameter β [Å^{-1}] fitted to $|H_{ab}| = Ae^{-\beta d/2}$ function. The values were calculated with PBE50/DZV and reoptimized 'Opt' basis set.

d [Å]	5.0	6.0	7.0	β [Å^{-1}]
DZV	47.8	22.0	5.1	2.24
Opt	92.0	27.3	7.8	2.47
Ref[a]	173.7	56.0	15.5	2.42

[a] CASSCF(3,8)/aug-cc-pVTZ values from Ref. 39

Table 3: Electronic coupling $|H_{ab}|$ values [meV] for organic-dimer HAB11 database molecules and the decay rate constants β [Å^{-1}] fitted to $H_{ab} = Ae^{-\beta d/2}$ expression.

Dimer	d [Å]	PBE	PBE0	PBE50	Ref.
Ethylene	3.5	380.1	427.5	474.6	519.2[a]
	4.0	183.5	217.6	253.7	270.8[a]
	4.5	89.2	111.6	137.1	137.6[a]
	5.0	43.1	56.9	73.3	68.5[a]
	β [Å^{-1}]	2.90	2.69	2.48	2.70
Acetylene	3.5	335.1	380.6	426.9	460.7[a]
	4.0	155.1	186.2	219.8	231.8[a]
	4.5	71.8	91.3	113.7	114.8[a]
	5.0	31.6	44.7	56.9	56.6[a]
	β [Å^{-1}]	3.14	2.86	2.68	2.80
Cyclopropene	3.5	383.5	438.7	496.9	536.6[a]
	4.0	177.0	213.1	253.8	254.0[a]
	4.5	80.0	102.3	129.1	118.4[a]
	5.0	35.7	48.8	65.5	54.0[a]
	β [Å^{-1}]	3.17	2.93	2.70	3.06
Cyclobutadiene	3.5	309.2	367.9	424.5	462.7[a]
	4.0	150.4	188.8	228.4	239.1[a]
	4.5	73.0	98.2	126.3	121.7[a]
	5.0	35.9	51.4	70.1	62.2[a]
	β [Å^{-1}]	2.87	2.62	2.40	2.67
Cyclopentadiene	3.5	329.5	380.9	436.4	465.8[a]
	4.0	159.0	193.3	232.4	234.4[a]
	4.5	77.6	99.7	126.3	114.3[a]
	5.0	37.7	51.5	69.1	53.4[a]
	β [Å^{-1}]	2.89	2.67	2.46	2.89
Furane	3.5	315.8	363.5	412.4	440.3[a]
	4.0	147.2	179.6	215.5	214.9[a]
	4.5	69.3	89.8	114.4	101.8[a]
	5.0	32.7	45.1	61.1	46.0[a]
	β [Å^{-1}]	3.02	2.78	2.54	3.01

Table 3: (*continued.*)

Dimer	d [Å]	PBE	PBE0	PBE50	Ref.
Pyrrole	3.5	328.1	376.6	425.2	456.3[a]
	4.0	156.3	190.0	226.5	228.6[a]
	4.5	75.5	97.3	123.0	111.3[a]
	5.0	36.6	50.0	67.2	52.2[a]
	β [Å^{-1}]	2.92	2.69	2.46	2.89
Thiophene	3.5	338.5	387.1	437.8	449.0[b]
	4.0	158.6	191.9	230.5	218.9[b]
	4.5	75.2	96.2	121.9	106.5[b]
	5.0	35.7	48.2	36.3	54.4[b]
	β [Å^{-1}]	3.00	2.78	3.24	2.82
Imidazole	3.5	309.2	353.9	406.5	411.6[b]
	4.0	144.4	176.5	211.1	202.6[b]
	4.5	68.2	60.7	110.3	99.1[b]
	5.0	32.3	24.3	39.9	49.7[b]
	β [Å^{-1}]	3.01	3.64	3.04	2.82
Benzene	3.5	332.4	377.0	428.1	435.2[b]
	4.0	154.1	186.4	223.2	214.3[b]
	4.5	43.2	92.7	118.0	104.0[b]
	5.0	5.0	44.2	61.0	51.7[b]
	β [Å^{-1}]	5.55	2.85	2.59	2.85
Phenol	3.5	254.9	289.3	324.9	375.0[b]
	4.0	114.4	136.5	160.8	179.6[b]
	4.5	52.4	66.3	81.5	85.2[b]
	5.0	22.9	30.2	42.1	41.3[b]
	β [Å^{-1}]	3.21	3.00	2.72	2.95

[a] MRCI+Q value from Reference 44
[b] NEVPT2 value from Reference 44

Table 4: Electronic coupling values [meV] from periodic-boundary calculations (PBC) of hole transfer between two oxygen vacancies in bulk MgO. Projection in POD was performed to D-A regions separated by one layer of atoms (R1) and to touching half-cell D-A regions (R2) for comparison. CDFT values were obtained with the R1 region definition.

	100	110	111
POD / R1	2.0	273.7	38.1
POD / R2	13.3	566.2	590.9
CDFT[a]	44.0	537.0	183.7

[a] Reference 60
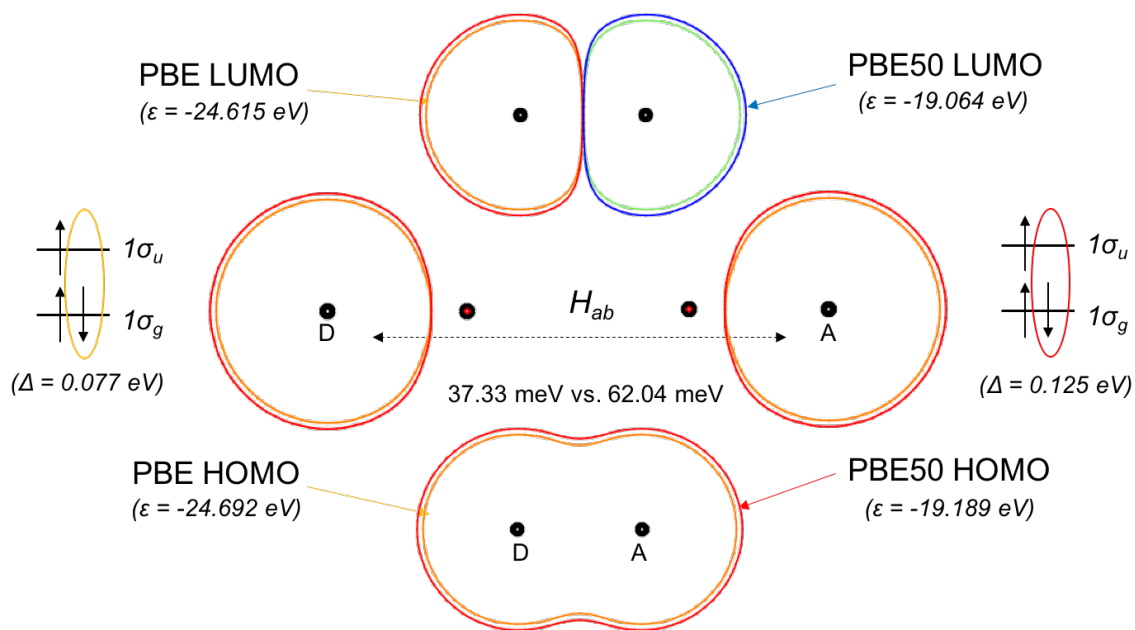
Figure 1: Effect of HFX in H_{ab} calculation on He_2^+ dimer at 3.0 Å. Highest occupied (HOMO) and lowest unoccupied (LUMO) adiabatic MOs of the He_2^+ are plotted at the bottom and top part of the figure, respectively, while the projected diabatic states localized on individual atoms are shown in the middle. Orbitals obtained by pure GGA are plotted in orange / green color while the PBE50 results are shown in red / blue. The $|H_{ab}|$ is proportional to the overlap of the diabatic states and have values of 37.33 meV (PBE) and 62.04 meV (PBE50).
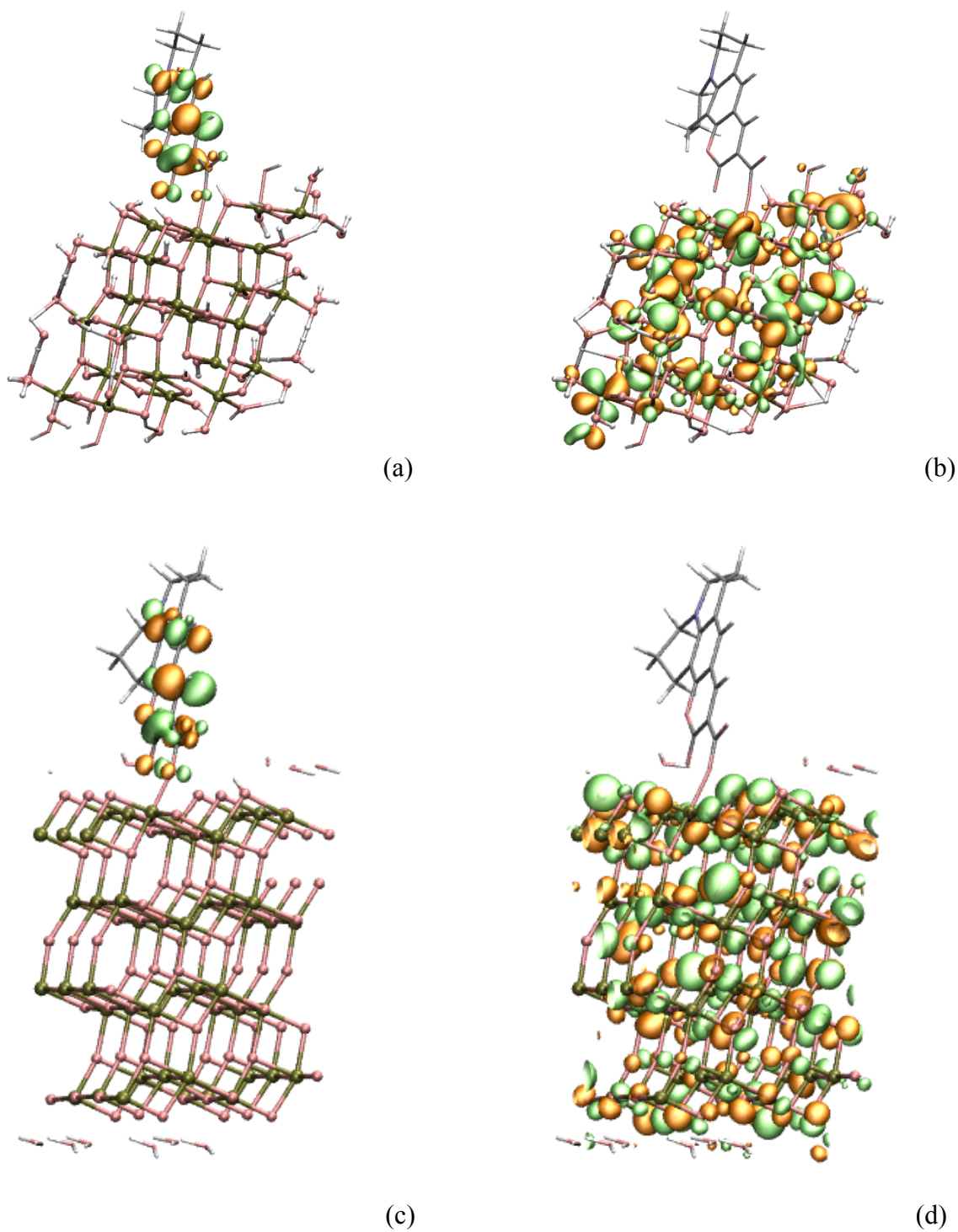
Figure 2: Structure of anatase TiO$_2$ cluster with adsorbed coumarine 343 molecule. (a) donor state molecular orbital in cluster model, (b) representative acceptor orbital on TiO$_2$, (c) donor state molecular orbital in surface model, and (d) representative acceptor orbital on TiO$_2$ surface are plotted.
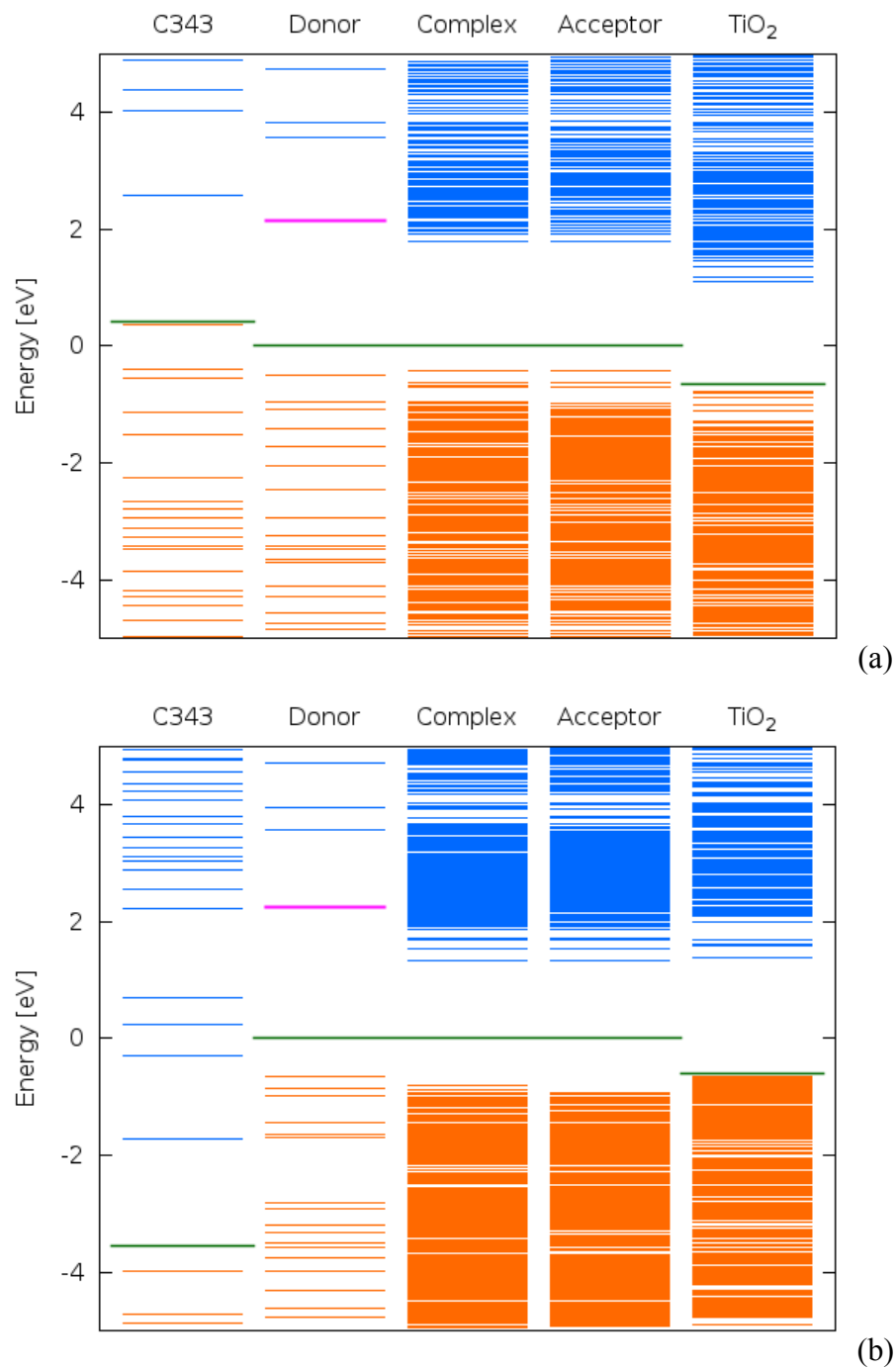
Figure 3: Electronic states of (a) TiO_2 cluster and (b) TiO_2 surface with adsorbed coumarine 343 molecule. The states of the whole system, denoted as 'complex', were decomposed to 'donor' part (C343) and 'acceptor' part (TiO_2) by the POD method. States of the isolated molecule and the titania cluster are shown for comparison. Donor state used for coupling element calculations is highlighted by magenta color, Fermi energy is shown by green line.

(a)

(b)
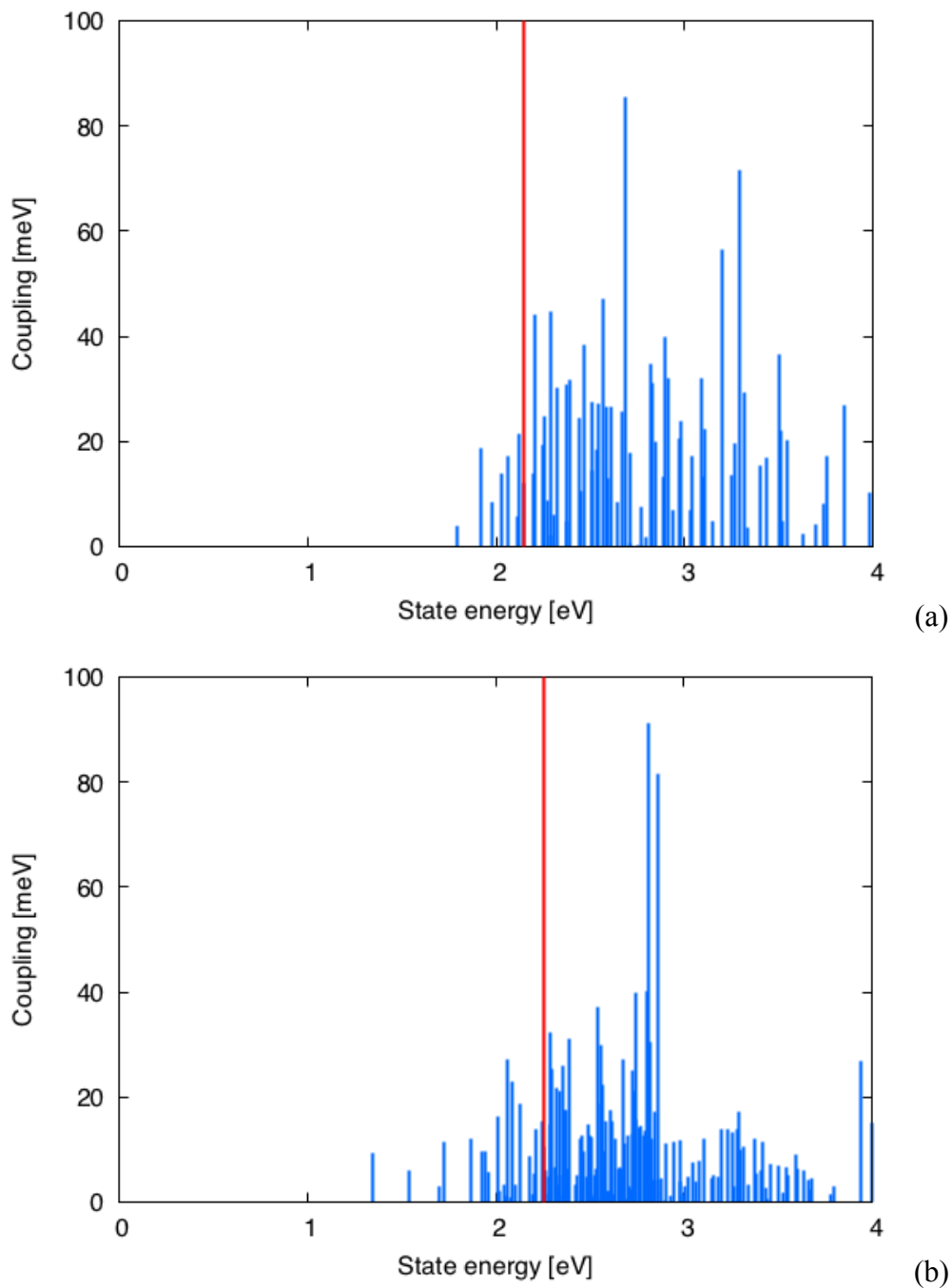
Figure 4: Magnitudes of the electronic coupling elements $|H_{ab}|$ between donor state localized on the coumarine and vacant states of (a) TiO_2 particle and (b) TiO_2 surface. Position of the donor state is marked by the red vertical line. The origin of the energy scale was aligned with the Fermi energy of the system.
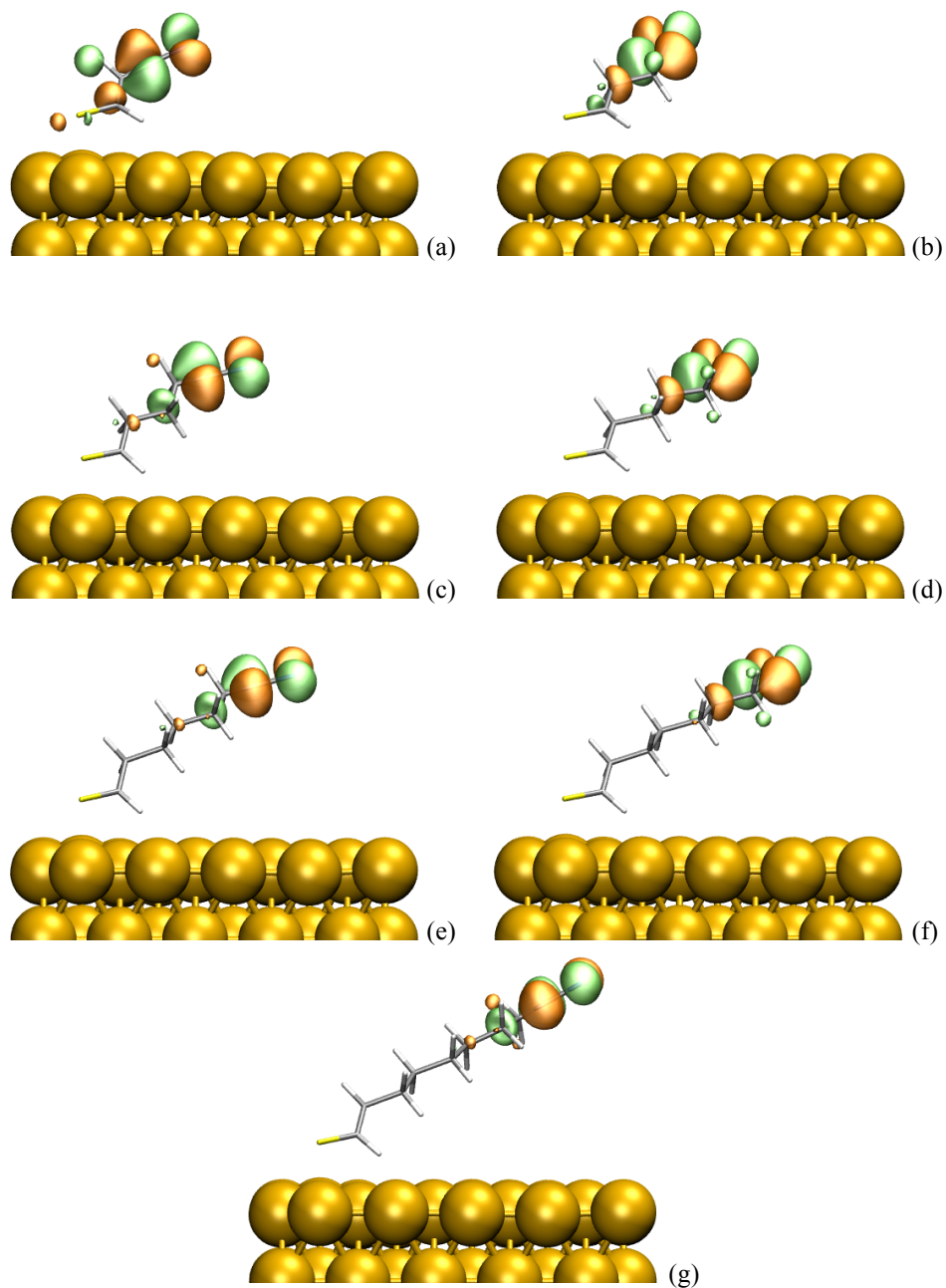
Figure 5: Localized π_1^* donor orbitals of (a) HCSCH$_2$CN, (b) HCS(CH$_2$)$_2$CN, (c) HCS(CH$_2$)$_3$CN, (d) HCS(CH$_2$)$_4$CN, (e) HCS(CH$_2$)$_5$CN, (f) HCS(CH$_2$)$_6$CN and (g) HCS(CH$_2$)$_7$CN molecule adsorbed on Au(111) surface.
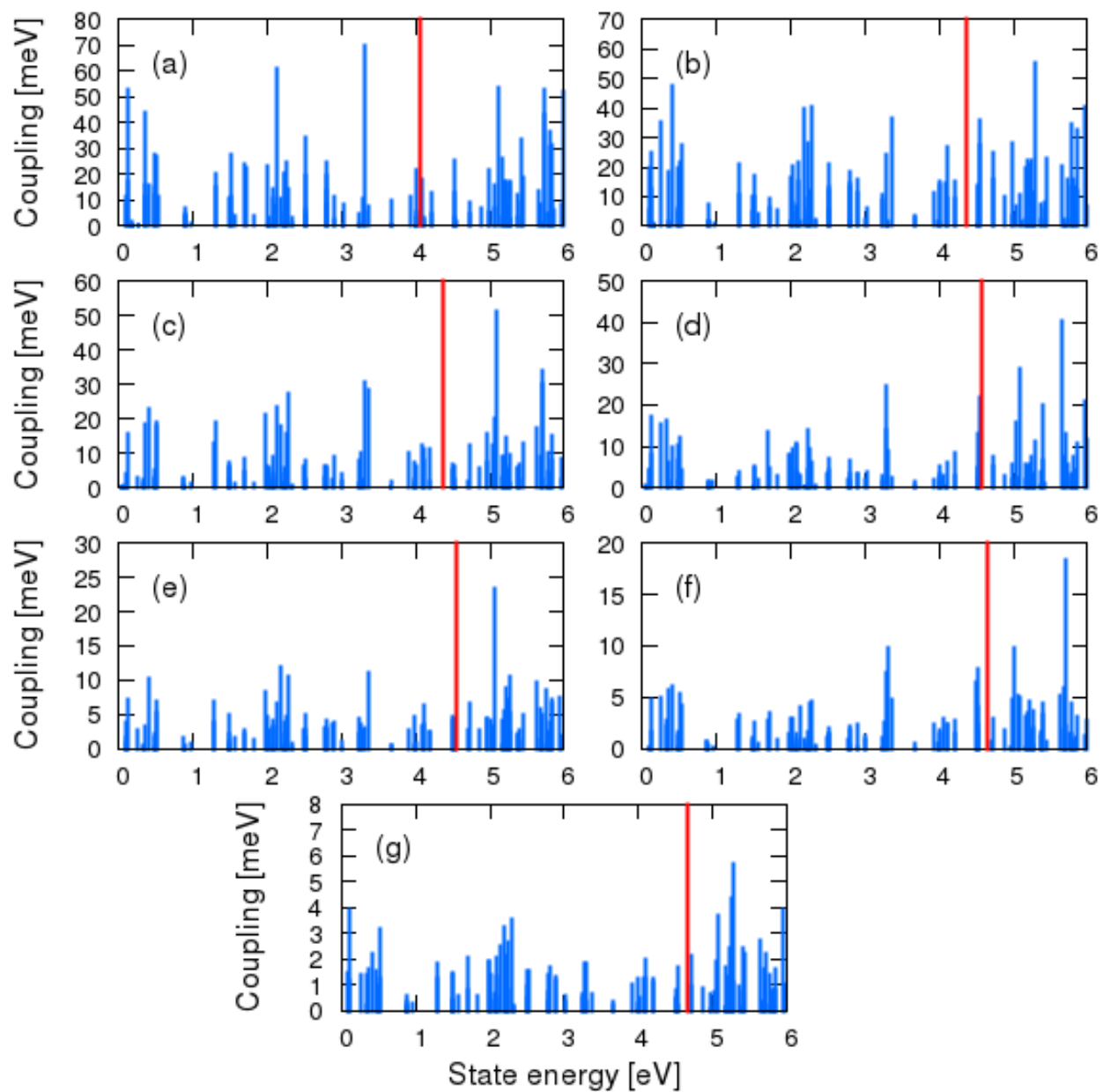
Figure 6: Values of the electronic coupling elements $|H_{ab}|$ between π_1^* donor state (red line) of (a) $HCSCH_2CN$, (b) $HCS(CH_2)_2CN$, (c) $HCS(CH_2)_3CN$, (d) $HCS(CH_2)_4CN$, (e) $HCS(CH_2)_5CN$, (f) $HCS(CH_2)_6CN$ and (g) $HCS(CH_2)_7CN$ molecule and Au(111) states. The origin of the energy scale is aligned with the Fermi level of the given system.
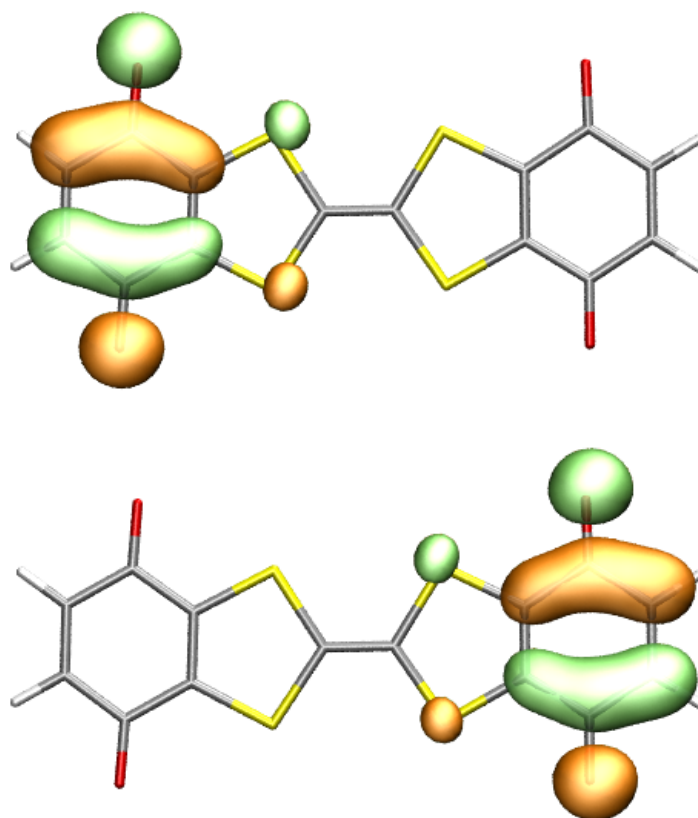
Figure 7: Diabatic states of the Q-TTF-Q$^-$ molecule obtained by the POD method using B3LYP functional and TVZP basis set. Donor-acceptor regions were defined as half of the molecule.

TOC Graphic